International Journal of Nanomedicine

Dovepress
open access to scientific and medical research

Open Access Full Text Article

ORIGINAL RESEARCH

Hydrogel-embedded nanocrystalline hydroxyapatite granules (elastic blocks) based on a cross-linked polyvinylpyrrolidone as bone grafting substitute in a rat tibia model

This article was published in the following Dove Press journal:
International Journal of Nanomedicine
12 October 2017
Number of times this article has been viewed

Michael Dau[1]
Cornelia Ganz[2]
Franziska Zaage[2]
Bernhard Frerich[1]
Thomas Gerber[2]

[1]Department of Oral, Maxillofacial and Plastic Surgery, University Medical Center Rostock, Rostock, Germany; [2]Institute of Physics, Rostock University, Rostock, Germany

Purpose: The aim of this study was to examine the in vivo characteristics and levels of integration and degradation of a ready-to-use bone grafting block with elastic properties (elastic block) for the use in surgery.

Materials and methods: Thirty-six male Wistar rats underwent surgical creation of a well-defined bone defect in the tibia. All created defects – one per animal – were filled with an unsintered nanocrystalline hydroxyapatite embedded either with a non-cross-linked hydrogel carrier (CONT, n=18) or a cross-linked hydrogel carrier (elastic block [EB], n=18) based on polyvinylpyrrolidone (PVP) and silica sol, respectively. The animals were killed after 12 (n=12), 21 (n=12) and 63 days (n=12). The bone formation and defect healing were quantified by histomorphometric measurements made in paraffin sections. Additionally, immunohistochemical (tartrate-resistant acid phosphatase [TRAP] and alkaline phosphatase [aP]), antibody-based examinations (CD68) and energy-dispersive x-ray scattering measurements of silica atom concentration were carried out.

Results: A larger remaining bone defect area overall was observed in EB after 12 days and 21 days. After 63 days, similar areas of remaining bone defects were found. The amount of the remaining carrier material in EB overall was higher at all times. In CONT no residual carrier material was found at 12 days and later. CD68 analyses showed significantly lower level of CD68-positive marked cells after 21 days in CONT, and nonsignificant differences at 12 and 63 days, respectively. Additionally, a significantly higher level of aP-positive marked cells was observed in CONT after 12 days. Later on, the levels of aP-positive marked cells were slightly higher in EB (21 and 63 days). Furthermore, no significant differences regarding the level of TRAP-positive marked cells in each group were observed.

Conclusion: The bone substitute (EB) with the cross-linked PVP-based hydrogel carrier leads at the beginning to a higher amount of remaining carrier material and remaining bone substitute. This delayed degradation is supposed to be the reason for the observed lower level of bone remodeling and is caused by the irradiation changes (cross links) in the structure in PVP.

Keywords: bone substitute, cross-linked, nanocrystalline hydroxyapatite, rat animal model, polyvinylpyrrolidone, irradiation, silica, osseointegration

Correspondence: Michael Dau
Department of Oral, Maxillofacial and Plastic Surgery, University Medical Center Rostock, Schillingallee 35, 18057 Rostock, Germany
Tel +49 381 494 6688
Fax +49 381 494 6698
Email michael.dau@med.uni-rostock.de

Introduction

The use of alloplastic bone substitute (BS) is one way to overcome the limitations – donor-site morbidity and the limited amount of available material[1–3] – of autologous

submit your manuscript | www.dovepress.com
Dovepress
http://dx.doi.org/10.2147/IJN.S142550

bone grafts, which are the first choice ("gold standard") because of their osteoconductive, osteoinductive and osteogenic properties.[3–6] However, no material was identified that compies with all optimum requirements.[7–9] There are various attempts to develop better alloplastic BSs and to find additional materials to improve the results regarding the bone regeneration. Next to the improvement of the bone remodeling itself, an easy handling for users is key to success. The main goal of clinical setting-focused research is the connection of easy handling of BSs with a reliable, quick bone regeneration. A starting point for improvement of the handling characteristic of biomaterials is the development of a new application form.[10] Shape builder is a method for improving bone remodeling because of the fact that it helps to avoid a very strong compression of the BS itself during application.[11] One approach is the use of polyvinylpyrrolidone (PVP) as an additional scaffold for granular BSs based on hydroxyapatite and silicon (Figure 1).[12] PVP is often used in pharmacology as a nanoparticle surface stabilizer, growth-affecting agent, as well as nanoparticle dispersing agent and reducing agent.[13] For the use in humans, nonautologous BS should be sterilized with the best available method before application. One of the most effective sterilization methods is gamma irradiation, but the sterilization process can influence the material properties of grafts.[14–17] Gamma irradiation is known to change the structure of PVP by inserting chain scission and cross-linking of polymers and behavior of PVP[18] by stabilization of the sol and hindering the condensation reaction on one hand. This irradiation can alter the molecular weight of the polymer, and, therefore, affect its mechanical properties and the rate at which it will degrade. On the other side, PVP reduces the collision possibility of particles in sol that is the cause of aggregation. According to Xu et al,[20] these two effects result in longer gelation time. But the biological effects on the bone formation following gamma irradiation of the PVP-based hydrogel carrier within the BS are unknown.

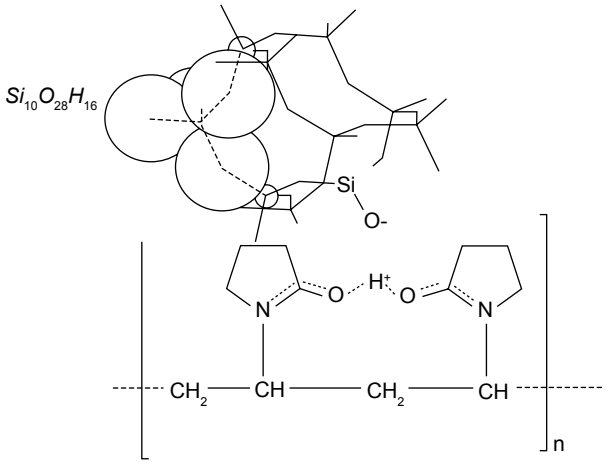

Figure 1 Structure of polyvinylpyrrolidone with central silicon dioxide.

The aim of this study was to evaluate the effects on bone remodeling in a rat animal model following the implantation of a nanocrystalline hydroxyapatite BS with an elastic cross-linked hydrogel carrier based on PVP (elastic block – EB).

Materials and methods

Study materials

Two BSs – based on a mixture of a synthetic unsintered nanocrystalline hydroxyapatite material embedded in a highly porous silica matrix in a ratio 61:39 (wt %) and an elastic hydrogel of PVP (Kollidon® 90, BASF SE, Ludwigshafen am Rhein, Germany; see Figure 1) – were examined in this study. The BSs were prepared of a 60 vol% adhesive hydrogel consisting of 6% PVP, 3% silica and 91% water mixed with 40 vol% of the above-described combination of a synthetic nanocrystalline hydroxyapatite material and silica matrix. One portion of this ready-to-use autoclaved mixture remained unaltered (non-cross-linked hydrogel carrier [CONT], NanoBone Putty, Artoss GmbH, Rostock, Germany), while the other portion (EB) underwent gamma irradiation by a $Cobalt^{60}$ source (Synergy Health Radeberg GmbH, Applied Sterilisation Technologies, Radeberg, Germany) at a dose rate of 25–40 kGy.

Animal model and procedures

An established animal rat tibia model was used in the present study.[19–21] The experiment was approved by University Medical Center Rostock, Germany (LVL M-V/TSD/7221.3–1.1–101/11) and followed the National Institutes of Health guidelines for the care and use of laboratory animals. Thirty-six male Wistar rats (average mean body weight: 465±33 g) were included in the study. The animals were kept at the laboratory with dry food and water ad libitum under standard conditions with an artificial light–dark cycle of 12 h each.

All surgical interventions were performed under general anesthesia with an intraperitoneal injected mixture of 40 mg ketamine hydrochloride (Ketamin® 10%, Belapharm, Vercha, Germany) and 3.5 mg xylazin hydrochloride (Rompun® 2%, Bayer HealthCare Animal Health, Leverkusen, Germany) per 400 mg animal. The median aspects of the tibias were exposed via tibial longitudinal incisions. A clear predefined 3.5-mm-diameter large monocortical and medullar defect (no significant difference between the two groups) was created on the proximal area of tibia using a dental drill bur 3F

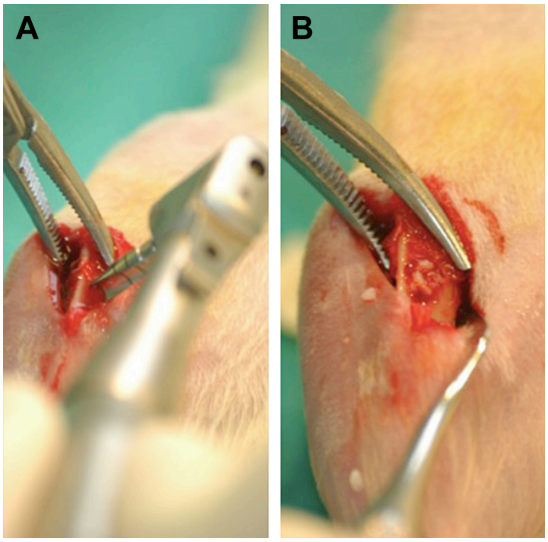

Figure 2 Intraoperative pictures.
Notes: (**A**) defect creation; (**B**) bone defect filled with bone substitute material.

(Figure 2A). Contact with cortical bone of the opposite side was strictly avoided. The cavities were randomly filled with the respective BSs (CONT: n=18; EB: n=18) (Figure 2B). Randomization was achieved using a computer-generated list. Periosteum, muscle and skin were closed in layers using absorbable suture material (Vicryl®, Ethicon, Norderstedt, Germany). Postoperatively, the animals received analgesics by applying 0.5 mg carprofenum (Rimadyl®, Zoetis Germany GmbH, Berlin, Germany) intramuscularly. Metamizol natrium (Novaminsulfon-ratiopharm®, ratiopharm GmbH, Ulm, Germany) was applied in the drinking water on a daily basis for the first 5 days postoperatively.

After 12, 21 and 63 days, the animals were killed by the intraperitoneal injection of 120 mg ketamine hydrochloride (Ketamin 10%, Belapharm, Vercha, Germany) and 10 mg xylazin hydrochloride (Rompun 2%, Bayer HealthCare Animal Health, Leverkusen, Germany) per 400 mg animal. The tibiae were harvested for further histological examination. The bones were fixed in 4% phosphate-buffered formalin for 7 days and subsequently decalcified in 20% ethylenediaminetetraacetic acid (pH 7.2–7.4) over a period of two weeks. Decalcified specimens were embedded in paraffin and 3-µm sections were cut and stained with Goldner's trichrome (Figure 3A) and hematoxylin–eosin (HE) (Figure 3B) for standard histological analysis, and tartrate-resistant acid phosphatase (TRAP) and CD68 for the evaluation of osteoclasts, respectively. For the measurement of osteoblast activity, additional specimens were stained with alkaline phosphatase (aP). Another section of each specimen was cut for microstructure analysis with scanning electron microscopy (SEM).

Histological analysis

The histological analysis was performed using a Zeiss light microscope (Axio Imager.M2 microscope, Zeiss, Oberkochen, Germany). The focus of the analysis was on the evaluation of the integration and degradation of the BS material as well as the bone formation and the remodeling process. The qualitative histological evaluation included the observation of the cells participating in the process of biomaterial integration and degradation, the development of newly formed bone, and the possible adverse reactions such as fibrotic encapsulation or necrosis. All histological figures were captured with a microscope camera (AxioCam MRc5 camera, Zeiss, Oberkochen, Germany) that was connected to an automatic scanning table (Scanningtisch M-686K011, Wienecke & Sinske GmbH, Gleichen, Germany).

Histomorphometrical measurements

The specimens (HE) were analyzed regarding newly formed bone, remaining BS, carrier material and soft tissue using Adobe Photoshop CS6 (Adobe Systems Inc., San Jose, CA,

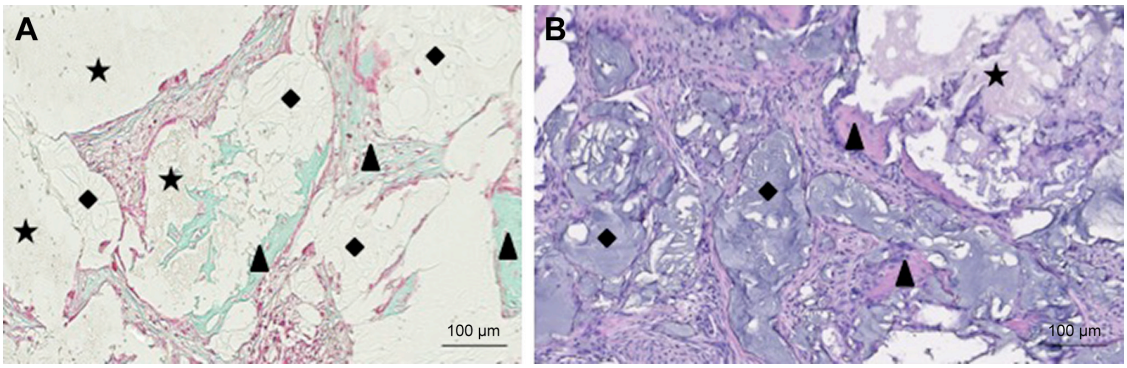

Figure 3 Histological figure in Goldner's trichrome staining (**A**) and hematoxylin–eosin (HE) staining (**B**).
Notes: (**A**) remaining bone substitute and newly-formed bone in EB at 21 days postoperatively (Goldner's trichrome staining); (**B**) remaining bone substitute and newly formed bone in EB at 21 days postoperatively (HE staining); scale bars: 100 µm. ★ Biomaterial; ▲ Newly-formed bone; ◆ Polymer PVP. Magnification ×20.

USA) software. To standardize the measurement two regions of interest were defined (Figure 4). The still visible defect line in the cortical bone was defined as lateral borders of the cortical defect area while the area is limited by the inner and outer lines of the cortical bone. Lateral borders of the medullary defect area were the extended visible defect line in the cortical bone. The outer border was the inner border of the cortical bone. The inner border was set by double width of the cortical bone height. The defect area overall was the combination of both areas described above.

These measurements were made on randomly chosen histology slides for each group (six animals per group and point in time) and expressed as ratio of surface area for the total defect (all) and limited to cortical defect area (cortical bone) and medullary defect area (bone marrow), respectively.

Additionally, the areas of CD68-, aP- and TRAP-positive marked cells were selected as sum of areas using Adobe Photoshop CS6 (Adobe Systems Inc., San Jose, CA, USA) software and measured for analyses. This selected area was set in relation to the whole defect area, and the ratio was described by percentage of the whole area. This analysis was only performed in the cortical bone area.

EDX analyses

EDX (energy-dispersive x-ray scattering) measurements of silica concentration were made in two randomly chosen animals in each group at every point of time. A scanning electron microscope (DSM960, Zeiss, Jena, Germany) was used to determine the local chemical composition of the BS. Cross sections of the tibia defect area were sputter-coated with a thin Au–Pd layer. Surface topography of the biomaterial was examined using an accelerating voltage of 10 kV. Quantitative results of chemical composition were determined with IDFix (IDFix version 7.9.0, SAMx, Trappes, France).

Statistics

All results in this study were expressed as arithmetic means ± standard error of the mean (SEM). Testing for statistical significance was done by nonparametric tests for dependent samples. Means were calculated, and bar charts were used for data illustration. Due to multiple testing for comparison of histological calculations (remaining BS, carrier material, soft tissue and newly formed bone), Bonferroni corrections were applied and p-values of ≤ 0.0166 or ≤ 0.0125 were seen as significant. However, p-values can be considered as descriptive only. All statistical analyses were performed using SPSS statistical package version 20.0 (SPSS Inc., Chicago, IL, USA).

Results

Results of histological analysis

Qualitative histological evaluation showed that both bone grafts were well tolerated and newly formed bone at different stages was found. At 12 and 21 days, the bone defect in both groups was still visible and the cortical bone gap was not closed. At the end point of observation, the bone gap was completely closed in BS with CONT. A remaining bone defect in EB (EB-like BS with cross-linked hydrogel carrier) was still found after 63 days. A continuous bone remodeling was observed at all points of time in both groups but the newly formed bone growth took place at a different speed in both groups. In CONT the polymer could not be detected at all times (Figures 5–7), while in EB the remaining carrier material was still found (Table 1, Figures 8–10). In both groups, aP-, TRAP- and CD68-positive marked cells were observed at all times (Figures 11–13). TRAP-positive marked cells were typically located around the BS material in CONT and EB and less around the cross-linked PVP in EB.

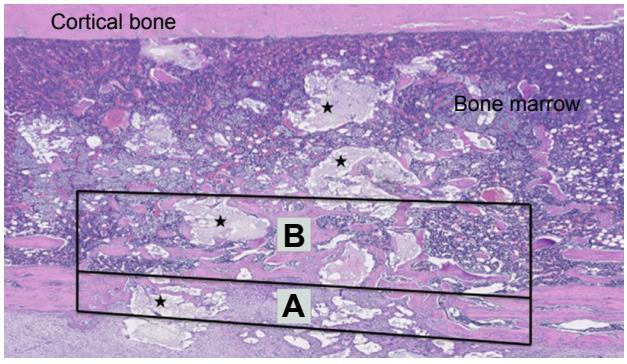

Figure 4 Defined areas of interest.
Notes: **A** cortical defect area; **B** medullary defect area; scale bars: 250 µm. Magnification ×5. ★ Biomaterial.

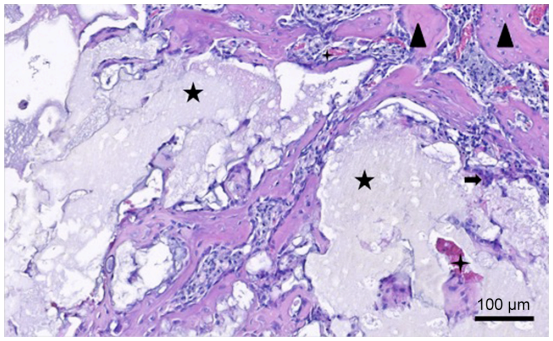

Figure 5 Histological figure in CONT at 12 days postoperatively.
Notes: Remaining bone substitute and newly-formed bone in CONT at 12 days postoperatively; scale bars: 100 µm. Magnification ×20. ★ Biomaterial; ▲ Newly-formed bone; ➡ Osteoclast; + Blood vessel.
Abbreviation: CONT, non-cross-linked hydrogel carrier.

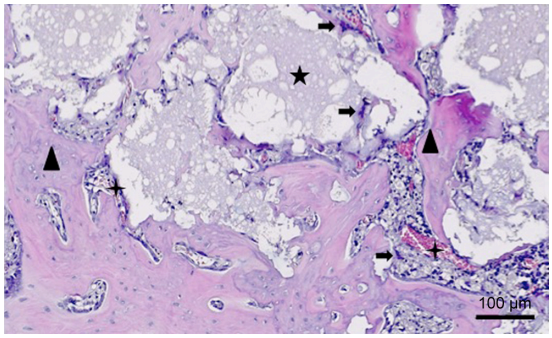

Figure 6 Histological figure in CONT at 21 days postoperatively.
Notes: Remaining bone substitute and newly-formed bone in CONT at 21 days postoperatively; scale bars: 100 µm. Magnification ×20. ★ Biomaterial; ▲ Newly-formed bone; ➡ Osteoclast; + Blood vessel.
Abbreviation: CONT, non-cross-linked hydrogel carrier.

The osteoblasts – found around the BS material and in small residual particles – were aP-positive, marked at different levels in both groups at various points of time.

At 12 days there was an organized fibrous tissue infiltration within and around the BS material in CONT (Figure 5). A degradation of the graft material was found as well as the bone ingrown at the borders of the defect next to the cortical bone. In EB, a less degradation of BS was observed while a similar bone ingrown at the defect bone borders was found (Figure 8). Within the defect area there was clearly recognizable bone regeneration around the implanted bone replacement material in both groups. Osteoblast seams, which characterize an active bone structure, newly formed blood vessels, connective tissue and some osteoclasts, and can be seen on the surface of the synthetic material, characterize the experimental period of 21 days (Figure 6). The cross-linked carrier material is clearly visible in the histological sections of EB after 21 days. Within the polymer, connective tissue can also be detected (Figure 9). At 63 days, histology looked similar in both groups while still an undirected bone structure was observed in the newly formed bone independent of the remaining or nonremaining bone defect. Areas of remaining BS with an ongoing bone remodeling were found in EB, while the bone remodeling in CONT was nearly accomplished. Besides these findings the histology looked very similar (Figures 7 and 10).

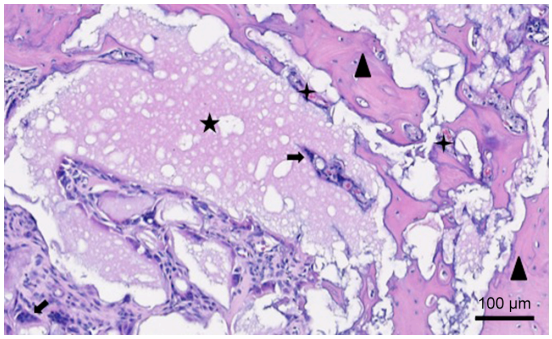

Figure 7 Histological figure in CONT at 63 days postoperatively.
Notes: Remaining bone substitute and newly-formed bone in CONT at 63 days postoperatively; scale bars: 100 µm. Magnification ×20. ★ Biomaterial; ▲ Newly-formed bone; ➡ Osteoclast; + Blood vessel.
Abbreviation: CONT, non-cross-linked hydrogel carrier.

Looking at the selected areas of CD68-positive marked cells in EB, a lower level (CONT: 17.5%+2.5% vs EB: 7.6%±1.2%; p=0.005; Table 2) was observed at 21 days. After 12 and 63 days no significant differences regarding the areas of CD68-positive marked cells within the two groups were found. Furthermore, no significant differences were found regarding the level of TRAP-positive marked cells at all points of time (Table 2). A significant higher level of aP-positive marked cells was observed in CONT after 12 days (CONT: 7.6%±1.4% vs EB: 1.3±0.4; p=0.006; Table 2). After 21 and 63 days, the level of aP-positive marked cells in CONT decreased and slightly higher levels were observed in EB at 21 days (CONT: 0.4%±0.1% vs EB: 1.8±0.6; p=0.091; Table 2) and 63 days (CONT: 0.9%±0.3% vs EB: 1.6±0.2; p=0.078; Table 2).

Results of histomorphometric analysis

The borders of the initially created cortical bone defects were clearly detectable in all animals and were used as a marker for histomorphometric analysis.

12 days

After 12 days, a significantly higher remaining bone defect (Table 1) was observed in CONT over all areas (CONT: 69.4%±2.2% vs EB: 91.9%±2.3%), in cortical bone area (CONT: 64.7%±3.1% vs EB: 89.7%±3.3%) and in medullary defect area (CONT: 71.9%±2.2% vs EB: 93.3%±1.8%). The amount of newly formed bone (Table 1) in EB is significantly lower in comparison to CONT over all areas (CONT: 30.6%±2.2% vs EB: 8.1%±2.3%), in cortical defect area (CONT: 35.3%±3.1% vs EB: 10.3%±3.3%; Figure 14) and in medullary defect area (CONT: 28.1%±2.2% vs EB: 6.7%±1.8%; Figure 15). No difference between the amount of remaining BS was found, but a significantly higher level of residual carrier material (Table 1) was observed in EB overall (30.1%±3.4%; Figure 16), in cortical defect area (19.5%±2.7%; Figure 14) and in medullary defect area (36.2%±4.9%; Figure 15). In CONT no remaining carrier material (Table 1) was detected.

21 days

A significantly higher remaining bone defect (Table 1) was found in EB over all areas (CONT: 65.4%±1.8%

Table 1 Overview for histomorphometrical measurement after 12, 21 and 63 days in CONT vs EB, mean (± SD)

	All areas			Cortical defect area			Medullary defect area		
	CONT	EB	*p*-value	CONT	EB	*p*-value	CONT	EB	*p*-value
12 days									
Remaining bone segment (BS) (%)	30.2 (±4.7)	28.9 (±4.2)	0.838	30.7 (±7.3)	30.1 (±6.8)	0.954	29.6 (±5.5)	28.8 (±4.6)	0.917
Carrier material (%)	0[a]	30.1 (±3.4)	<0.0001	0[a]	19.5 (±2.7)	<0.0001	0[a]	36.2 (±4.9)	<0.0001
Soft tissue (%)	39.2 (±4.0)	32.9 (±3.3)	0.258	34.0 (±5.4)	40.0 (±5.6)	0.459	42.3 (±5.5)	28.2 (±2.9)	0.047
Newly formed bone (%)	30.6 (±2.2)	8.1 (±2.3)	<0.0001	35.3 (±3.1)	10.3 (±3.3)	<0.0001	28.1 (±2.2)	6.7 (±1.8)	<0.0001
21 days									
Remaining BS (%)	27.2 (±1.8)	19.4 (±2.9)	0.046	30.4 (±4.6)	16.0 (±3.1)	0.026	25.8 (±1.6)	21.4 (±4.5)	0.382
Carrier material (%)	0[a]	33.0 (±6.4)	<0.0001	0[a]	27.9 (±6.5)	0.002	0[a]	36.1 (±6.8)	<0.0001
Soft tissue (%)	38.2 (±2.5)	33.3 (±3.7)	0.307	26.6 (±4.8)	32.0 (±5.2)	0.461	41.6 (±3.6)	33.9 (±3.3)	0.147
Newly formed bone (%)	34.6 (±1.8)	14.3 (±3.6)	0.001	43.0 (±3.3)	24.0 (±5.3)	0.012	32.7 (±3.6)	8.6 (±3.1)	<0.0001
63 days									
Remaining BS (%)	21.8 (±2.7)	19.2 (±4.4)	0.620	18.2 (±1.4)	13.7 (±4.4)	0.359	23.7 (±3.7)	22.2 (±4.9)	0.816
Carrier material (%)	0[a]	25.5 (±3.8)	<0.0001	0[a]	20.0 (±3.7)	<0.0001	0[a]	28.6 (±4.5)	<0.0001
Soft tissue (%)	41.3 (±4.2)	22.2 (±2.3)	0.002	11.1 (±2.1)	14.4 (±2.1)	0.295	57.4 (±6.0)	26.9 (±4.0)	0.002
Newly formed bone (%)	36.9 (±2.3)	33.1 (±4.9)	0.495	70.7 (±2.6)	51.8 (±6.5)	0.022	18.9 (±2.6)	22.3 (±4.9)	0.562

Notes: Histomorphometrical measurement after 12, 21 and 63 days for CONT vs EB (standard error of the mean); [a]Not detectable; Analysis-of-variance test with Bonferoni correction significant level at $p<0.0125$.
Abbreviations: CONT, non-cross-linked hydrogel carrier; EB, elastic block.

vs EB: 85.7%±3.6%; $p=0.001$; Figure 16), in cortical defect area (CONT: 57.0%±3.3% vs EB: 76.0%±5.3%; $p=0.012$; Figure 14) and in medullary defect area (CONT: 67.3%±3.6% vs EB: 91.4%±3.1%; Figure 15). Overall the amount of newly formed bone (Table 1) in EB is significantly lower in comparison to CONT (CONT: 34.6%±1.8% vs EB: 14.3%±3.6%; Figure 16) as well as in cortical defect area (CONT: 43.0%±3.3% vs EB: 24.0±5.3%; $p=0.012$; Figure 14) and in medullary defect area (CONT: 32.7%±3.6% vs EB: 8.6%±3.1%; Figure 15). Regarding the remaining BS, no significant differences were found at this point of time (Table 1). Higher amounts of residual carrier material (Table 1) were observed in EB overall (33.0%±6.4%; Figure 10), in cortical defect area (27.9%±6.5%; Figure 14) and in medullary defect area (36.1%±6.8%; Figure 15), while in CONT no remaining carrier material was detected.

63 days

After 63 days, no difference regarding the remaining bone defect (Table 1) was observed in EB over all areas (CONT: 63.1%±2.3% vs EB: 66.9%±4.9%; Figure 16) and in medullary defect area (CONT: 81.1%±2.6% vs EB: 77.7%±4.9%; Figure 15). In the cortical defect area (CONT: 29.3%±2.6%; Figure 14) no significant difference in residual bone defect was found but a trend was detected. The amount of newly

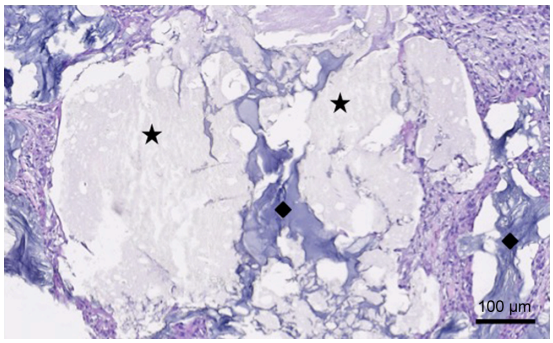

Figure 8 Histological figure in EB at 12 days postoperatively.
Notes: Remaining bone substitute and newly-formed bone in EB at 12 days postoperatively; scale bars: 100 µm. Magnification ×20. ★ Biomaterial; ◆ Polymer PVP.
Abbreviation: EB, elastic block.

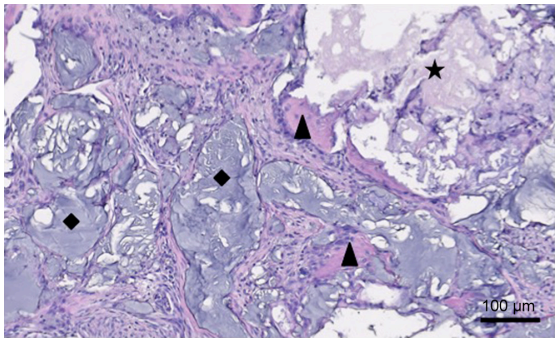

Figure 9 Histological figure in EB at 21 days postoperatively.
Notes: Remaining bone substitute and newly-formed bone in EB at 21 days postoperatively; scale bars: 100 µm. Magnification ×20. ★ Biomaterial; ▲ Newly-formed bone; ◆ Polymer PVP.
Abbreviation: EB, elastic block.

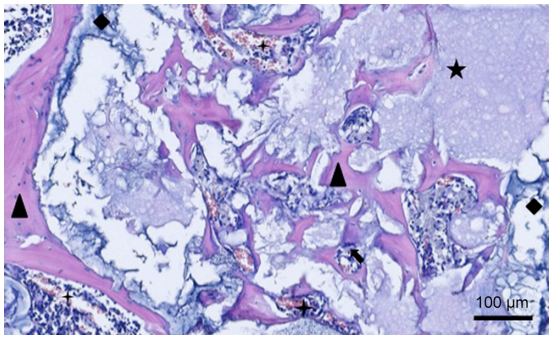

Figure 10 Histological figure in EB at 63 days postoperatively.
Notes: Remaining bone substitute and newly-formed bone in EB at 63 days postoperatively; scale bars: 100 µm. Magnification ×20. ★ Biomaterial; ▲ Newly-formed bone; ➡ Osteoclast; + Blood vessel; ◆ Polymer PVP.
Abbreviation: EB, elastic block.

formed bone (Table 1) in EB showed no significant difference in comparison to CONT overall areas (CONT: 36.9%±2.3% vs EB: 33.1%±4.9%; Figure 16) and in medullary defect area (CONT: 18.9%±2.6% vs EB: 22.3%±4.9%; Figure 15) but a slight nonsignificant trend in cortical defect area (CONT: 70.7%±2.6% vs EB: 51.8%±6.5%; Figure 14). No differences in the detected amount of remaining BS were detected at this point of time (Table 1). But a higher amount of residual carrier material (Table 1) was observed in EB overall (25.5%±3.8%; Figure 16), in cortical defect area (20.0%±3.7%; Figure 14) and in medullary defect area (28.6%±4.5%; Figure 15), while in CONT no remaining carrier material was detected.

EDX analyses

The investigation of the composition change of the used material was performed by EDX analysis. These analyses of bone grafting granules within the BS with the CONT and the cross-linked carrier (EB-like BS with cross-linked hydrogel carrier) showed a similar silica concentration after 12 days (Figure 17). After 21 days, the silicon contents differed significantly from each other. While only 5.4±4.4 (wt) % silicon could be detected in CONT, the value in EB was 16.8±5.1 (wt) %. Nevertheless, the granules in the group with the cross-linked carrier showed a considerable decrease of silicon content after 63 days. Both contents were under 1 (wt) % (CONT: 0.3%±0.1% vs EB: 0.5%±0.3%).

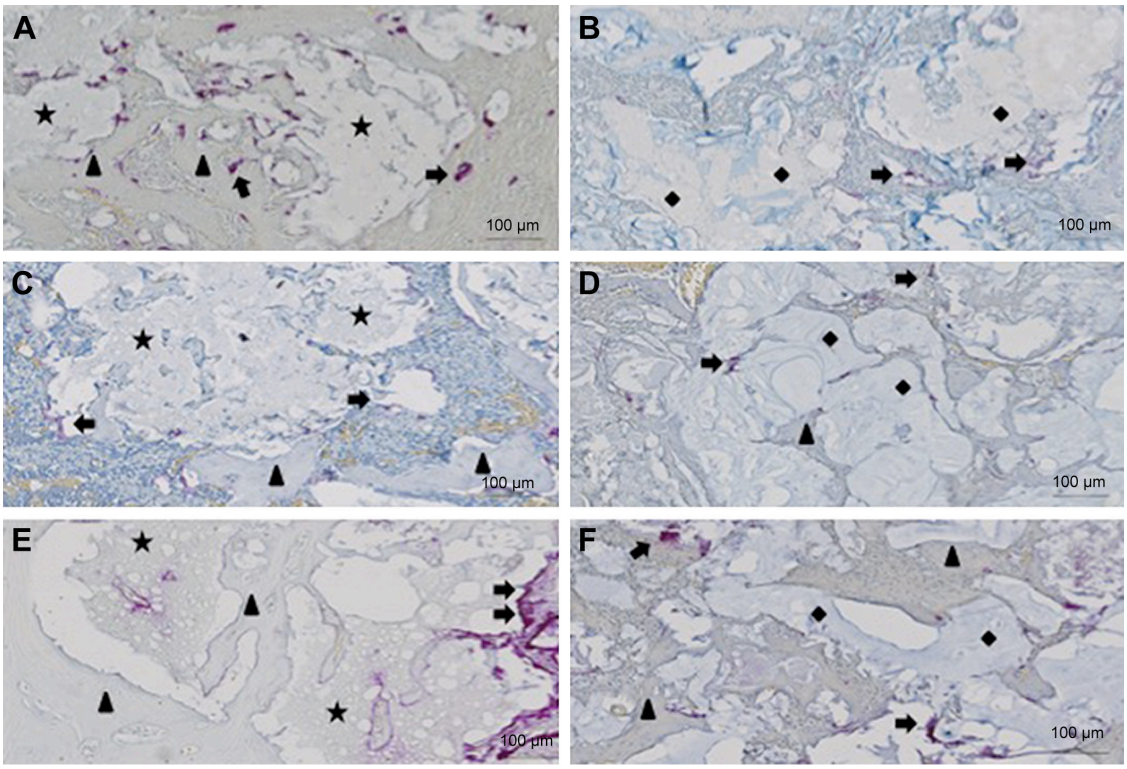

Figure 11 CD68-positive marked cells in CONT and EB at different points of time.
Notes: TRAP-positive marked cells in CONT (**A**, **C**, **E**) and EB at time points (**B**, **D**, **F**) at time points 12 (**A** vs **B**), 21 (**C** vs **D**) and 63 days postoperatively (**E** vs **F**); scale bars: 100 µm. Magnification ×20. ★ Biomaterial; ▲ Newly-formed bone; ◆ Polymer PVP; ➡ TRAP-positive marked cells.
Abbreviations: CONT, non-cross-linked hydrogel carrier; EB, elastic block; TRAP, tartrate-resistant acid phosphatase.

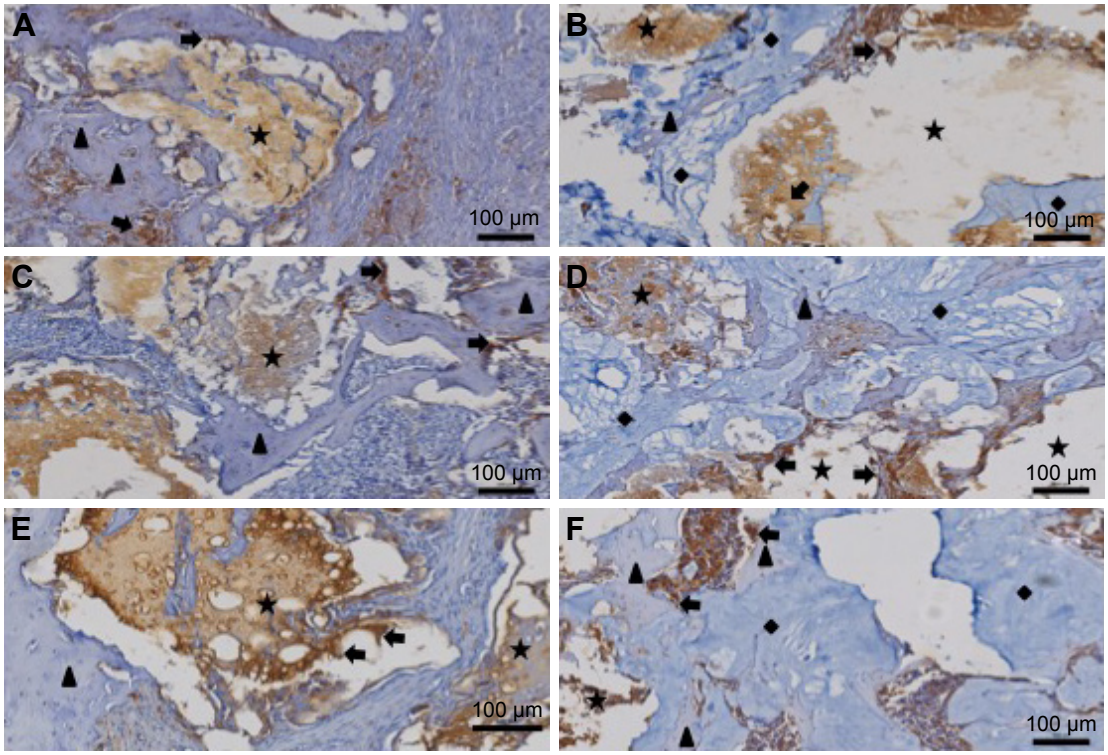

Figure 12 TRAP-positive marked cells in CONT and EB at different points of time.
Notes: CD68-positive marked cells in CONT (**A**, **C**, **E**) and EB (**B**, **D**, **F**) at time points 12 (**A** vs **B**), 21 (**C** vs **D**) and 63 days (**E** vs **F**) postoperatively; scale bars: 100 µm. Magnification ×20. ★ Biomaterial; ▲ Newly-formed bone; ◆ Polymer PVP; ➡ CD68-positive marked cells.
Abbreviations: CONT, non-cross-linked hydrogel carrier; EB, elastic block; TRAP, tartrate-resistant acid phosphatase.

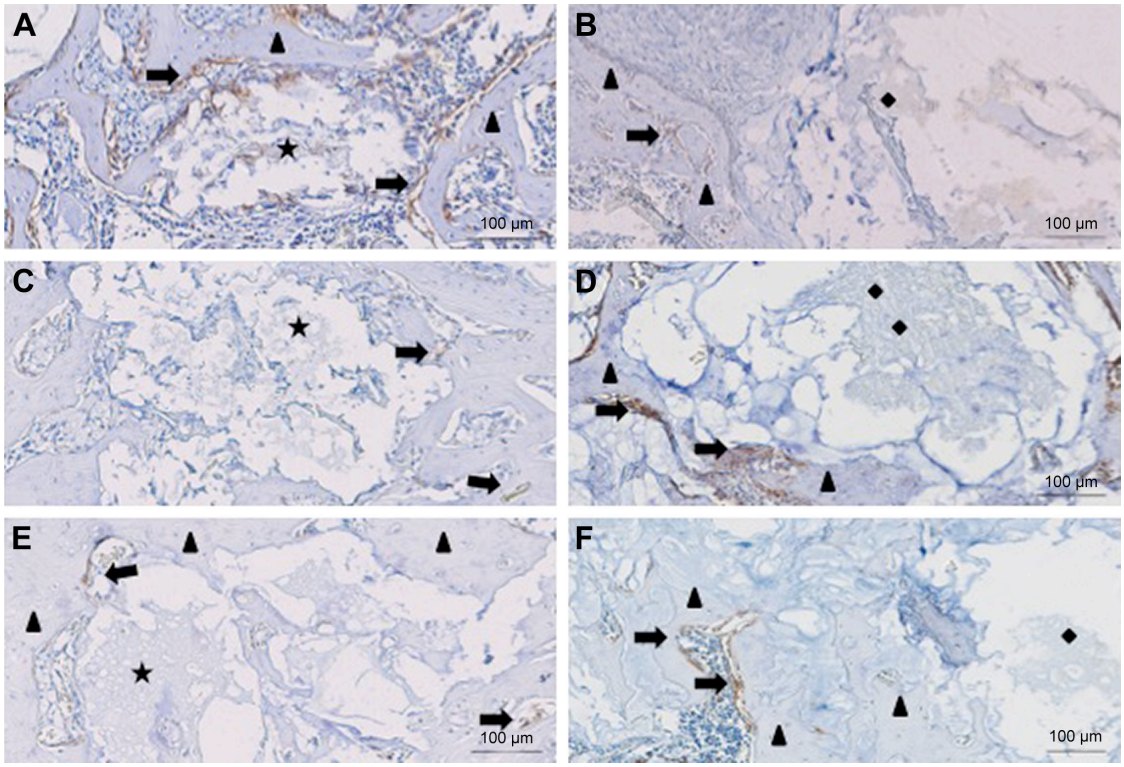

Figure 13 Alkaline phosphatase (aP)-positive marked cells in CONT (**A**, **C**, **E**) and EB (**B**, **D**, **F**) at time points 12 (**A** vs **B**), 21 (**C** vs **D**) and 63 days (**E** vs **F**) postoperatively; scale bars: 100 µm. Magnification ×20. ★ Biomaterial; ▲ Newly-formed bone; ◆ Polymer PVP; ➡ aP-positive marked cells.
Abbreviations: CONT, non-cross-linked hydrogel carrier; EB, elastic block.

Table 2 Measurement of CD68-positive and TRAP-positive marked cells in percentage after 12, 21 and 63 days, respectively, in CONT vs EB, mean (± SD)

	CD68-positive marked area in percentage			TRAP-positive marked area in percentage			Alkaline phosphatase-positive marked area in percentage		
	CONT	EB	*p*-value	CONT	EB	*p*-value	CONT	EB	*p*-value
12 days	31.1 (±7.1)	16.9 (±5.1)	0.131	3.1 (±1.1)	1.0 (±0.6)	0.167	7.6 (±1.4)	1.3 (±0.4)	0.006
21 days	17.5 (±2.5)	7.6 (±1.2)	0.005	0.2 (±0.1)	1.0 (±0.4)	0.062	0.4 (±0.1)	1.8 (±0.6)	0.091
63 days	11.1 (±1.9)	10.1 (±2.7)	0.78	1.2 (±0.5)	0.6 (±0.4)	0.354	0.9 (±0.3)	1.6 (±0.2)	0.078

Notes: Areas of CD68-positive, TRAP-positive alkaline phosphatase-positive marked cells in percentage after 12, 21 and 63 days, respectively, for CONT vs EB (standard error of the mean); Analysis-of-variance test with significant level of $p<0.05$.
Abbreviations: CONT, non-cross-linked hydrogel carrier; EB, elastic block; TRAP, tartrate-resistant acid phosphatase.

Discussion

The aim of the study was to examine the in vivo characteristics and levels of integration and degradation of a ready-to-use bone grafting block with elastic properties (EB) for the use in surgery. In the presented study, a significant influence of the cross-linked carrier material on the bone remodeling was found. Irradiation of BSs influences the material properties of grafts,[14–17] which in turn can affect the process of bone formation, bony consolidation and bone remodeling.[22–25] Significant differences in the tested groups – BS with CONT and BS with cross-linked carrier material (EB) – were found over all points in time. A lower degradation rate of the BS was detected in the group with the cross-linked hydrogel carrier (EB). The slowing down in degradation was not caused by the BS itself but rather by the cross-linked PVP material serving as a shape builder. The observed structural changes of PVP following gamma irradiation in an earlier study[18] might have suggested such an impact but were not proven till today. In literature a delayed in vivo degradation of complex molecules like poly-L-lactide after irradiation is described,[25] while irradiation of hydroxyapatite showed no chemical degradation, structural change or effects on bone remodeling.[26,27] Therefore, the nonirradiated BS with the non-cross-linked elastic hydrogel PVP carrier and the gamma-irradiated synthetic nanostructured BS with the cross-linked elastic hydrogel PVP carrier were compared in vivo by means of their soft and hard tissue responses, the immunological fluorescence examination and the EDX analyses. A delayed degradation of the cross-linked hydrogel carrier with a slowing-down effect on the bone remodeling was found. Additionally, a prolonged detection time of silica was observed, which

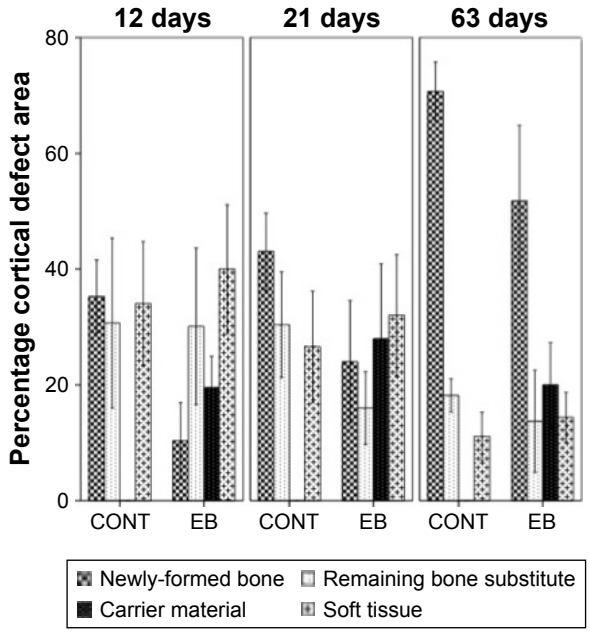

Figure 14 Bar chart of remaining bone substitute, remaining carrier material, soft tissue and newly formed bone in percentage in cortical defect area at different points of time in CONT and EB.
Abbreviations: CONT, non-cross-linked hydrogel carrier; EB, elastic block.

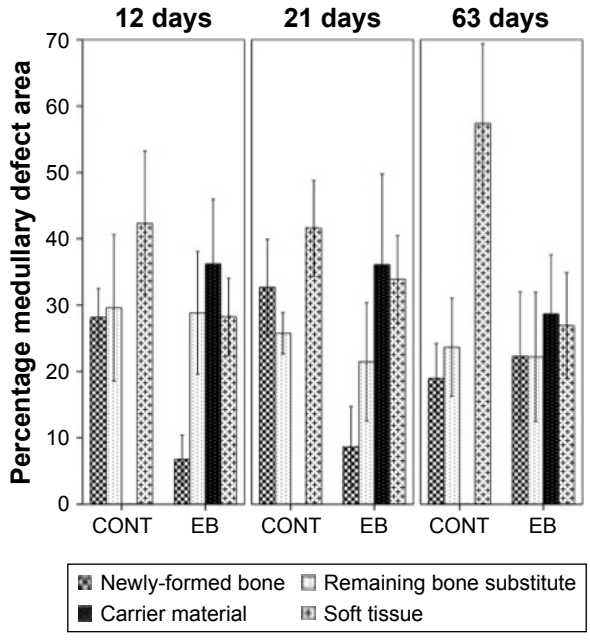

Figure 15 Bar chart of remaining bone substitute, remaining carrier material, soft tissue and newly formed bone in percentage in medullary defect area at different points of time in CONT and EB.
Abbreviations: CONT, non-cross-linked hydrogel carrier; EB, elastic block.

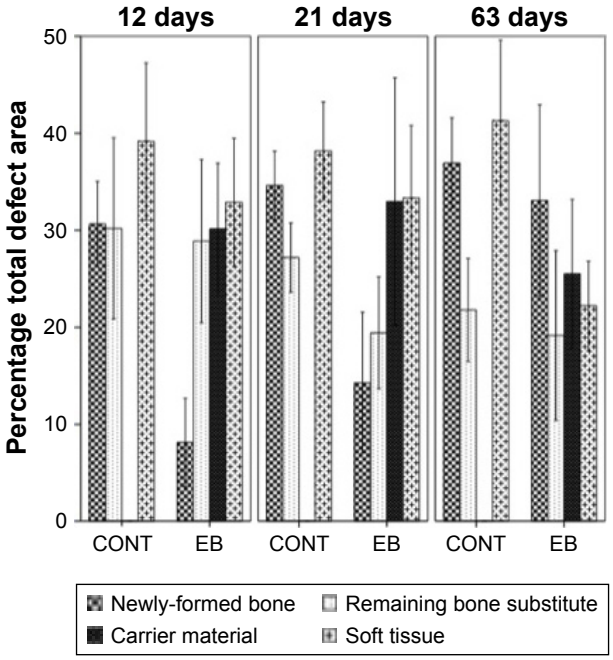

Figure 16 Bar chart of remaining bone substitute, remaining carrier material, soft tissue and newly formed bone in percentage in total defect area at different points of time in CONT and EB.
Abbreviations: CONT, non-cross-linked hydrogel carrier; EB, elastic block.

might be a side effect of the slow degradation of the surrounding cross-linked elastic hydrogel carrier. Xu et al found a prolonged detection of silicon dioxide too but stated that the observed changes in the fractal dimensions of PVP/SiO_2 sols explained the different microstructures of SiO_2 sol particles in the presence of PVP.[18] While trying to develop better biomaterials it should be kept in mind that every additional material for improving the biomaterial can change the material properties[28,29] and might have its own limitations and disadvantages.[30] For the tested nanocrystalline hydroxyapatite BS with an elastic hydrogel carrier based on PVP, a significant slower degradation of the BS with the cross-linked PVP carrier – created by irradiation – was observed. This led to lower amount of newly formed bone in the early phases (EB). After 63 days the values regarding the amount of remaining BS and newly formed bone were similar. As a result of the fact that the remains of the tested BSs were found even after 63 days, future research should extend the maximum observation time to study long-time effects regarding the degeneration of the tested cross-linked PVP.

Conclusion

At the beginning there was a significant decreased amount of newly formed bone, a significant increased amount of remaining BS and higher level of remaining carrier material in BS group with the cross-linked hydrogel carrier (EB). Later a similar bone remodeling was observed. This delayed bone remodeling is caused by changes of the structure of PVP (cross linking) because of the gamma irradiation. In conclusion, the modification of the hydrogel carrier by irradiation leads to a better clinical handling but disrupts the bone remodeling based on a delayed resorption of the cross-linked hydrogel carrier (PVP).

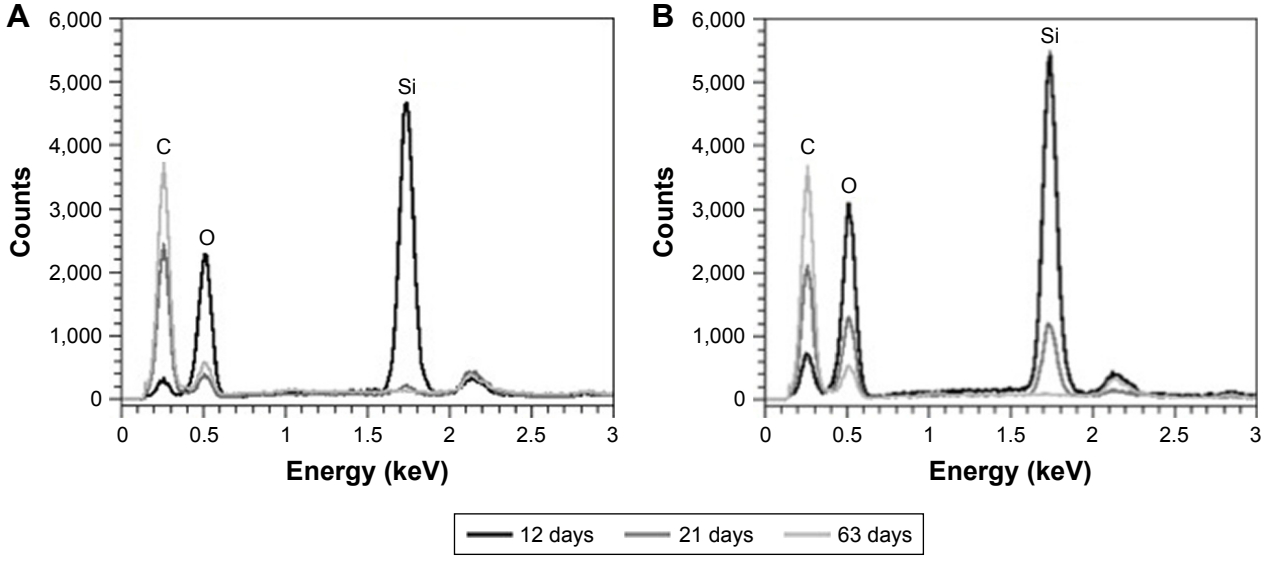

Figure 17 Line chart of silicon concentration in remaining bone substitute (**A**) CONT; (**B**) EB at different points of time.
Abbreviations: CONT, non-cross-linked hydrogel carrier; EB, elastic block.

Acknowledgments

We thank Daniel Wolter for excellent technical assistance. This research did not receive any specific grant from funding agencies in the public, commercial, or not-for-profit sectors.

Author contributions

BF and TG carried out the conception and design of the study. MD and CG organized and supervised animal experiments, the measurements and the collection of the data. MD did the animal experiments. MD and FZ did the measurements of the histopathologic specimens. MD did the immunohistochemical measurements. FZ did the energy-dispersive x-ray scattering (EDX) analyses. MD, CG and FZ analyzed the data, did the statistics and drafted the manuscript. MD, BF, FZ, CG and TG conducted the interpretation of the data.

All authors contributed toward data analysis, drafting and revising the paper and agree to be accountable for all aspects of the work.

Disclosure

TG is a member of the executive committee of Artoss GmbH, Rostock, Germany, and has been part of the group that developed NanoBone® elastic block. The other authors declare that they have no conflicts of interest and financial interests related to any products involved in this study.

References

1. Dimitriou R, Mataliotakis GI, Angoules AG, Kanakaris NK, Giannoudis PV. Complications following autologous bone graft harvesting from the iliac crest and using the RIA: a systematic review. *Injury*. 2011;42(Suppl 2):S3–S15.
2. Schwartz CE, Martha JF, Kowalski P, et al. Prospective evaluation of chronic pain associated with posterior autologous iliac crest bone graft harvest and its effect on postoperative outcome. *Health Qual Life Outcomes*. 2009;7:49.
3. Sen MK, Miclau T. Autologous iliac crest bone graft: should it still be the gold standard for treating nonunions? *Injury*. 2007;38(Suppl 1):S75–S80.
4. Finkemeier CG. Bone-grafting and bone-graft substitutes. *J Bone Joint Surg Am*. 2002;84-A(3):454–464.
5. Gazdag AR, Lane JM, Glaser D, Forster RA. Alternatives to autogenous bone graft: efficacy and indications. *J Am Acad Orthop Surg*. 1995;3(1):1–8.
6. Khan SN, Cammisa FP Jr, Sandhu HS, Diwan AD, Girardi FP, Lane JM. The biology of bone grafting. *J Am Acad Orthop Surg*. 2005;13(1):77–86.
7. Fanghanel J. Biomechanics and biomaterials in oral rehabilitation and dental treatment. *Biomed Tech (Berl)*. 2008;53(5):213–214.
8. Klein MO, Al-Nawas B. For which clinical indications in dental implantology is the use of bone substitute materials scientifically substantiated? (Systematic review, consensus statements and recommendations of the 1st DGI Consensus Conference in September 2010, Aerzen, Germany). *Eur J Oral Implantol*. 2011;4:S11–S29.
9. Hammerle CH, Jung RE. Bone augmentation by means of barrier membranes. *Periodontol 2000*. 2003;33:36–53.
10. Ruffieux K. A new syringe-delivered, moldable, alloplastic bone graft substitute. *Compend Contin Educ Dent*. 2014;35(4 Suppl):8–10.
11. Vance GS, Greenwell H, Miller RL, Hill M, Johnston H, Scheetz JP. Comparison of an allograft in an experimental putty carrier and a bovine-derived xenograft used in ridge preservation: a clinical and histologic study in humans. *Int J Oral Maxillofac Implants*. 2004;19(4):491–497.
12. Gerber T, Ganz C, Xu W, Maier B, Frerich B, Lenz S. Bone grafting putty – animal experiments and clinical applications. *Key Eng Mater*. 2012;529–530:285–290.
13. Koczkur KM, Mourdikoudis S, Polavarapu L, Skrabalak SE. Polyvinylpyrrolidone (PVP) in nanoparticle synthesis. *Dalton Trans*. 2015;44(41):17883–17905.
14. Currey JD, Foreman J, Laketic I, Mitchell J, Pegg DE, Reilly GC. Effects of ionizing radiation on the mechanical properties of human bone. *J Orthop Res*. 1997;15(1):111–117.
15. DePaula CA, Truncale KG, Gertzman AA, Sunwoo MH, Dunn MG. Effects of hydrogen peroxide cleaning procedures on bone graft osteoinductivity and mechanical properties. *Cell Tissue Bank*. 2005;6(4):287–298.
16. Gibbons MJ, Butler DL, Grood ES, Bylski-Austrow DI, Levy MS, Noyes FR. Effects of gamma irradiation on the initial mechanical and material properties of goat bone-patellar tendon-bone allografts. *J Orthop Res*. 1991;9(2):209–218.
17. Salehpour A, Butler DL, Proch FS, et al. Dose-dependent response of gamma irradiation on mechanical properties and related biochemical composition of goat bone-patellar tendon-bone allografts. *J Orthop Res*. 1995;13(6):898–906.
18. Xu Y, Wu D, Sun Y, et al. Effect of polyvinylpyrrolidone on the ammonia-catalyzed sol–gel process of TEOS: Study by in situ 29Si NMR, scattering, and rheology. *Colloids Surf A*. 2007;305(1–3):97–104.
19. Ganz C, Xu W, Holzhüter G, Götz W, Vollmar B, Gerber T. Comparison of bone substitutes in a tibia defect model in Wistar-rats. *Key Eng Mater*. 2012;493–494:732–738.
20. Xu W, Ganz C, Weber U, et al. Evaluation of injectable silica-embedded nanohydroxyapatite bone substitute in a rat tibia defect model. *Int J Nanomedicine*. 2011;6:1543–1552.
21. Zaage F, Dau M, Ganz C, Frerich B, Gerber T. Elastic blocks: hydrogel-embedded granules as bone grafting substitutes. *Key Eng Mater*. 2015;631:414–419.
22. Busenlechner D, Tangl S, Mair B, et al. Simultaneous in vivo comparison of bone substitutes in a guided bone regeneration model. *Biomaterials*. 2008;29(22):3195–3200.
23. Dau M, Kammerer PW, Henkel KO, Gerber T, Frerich B, Gundlach KK. Bone formation in mono cortical mandibular critical size defects after augmentation with two synthetic nanostructured and one xenogenous hydroxyapatite bone substitute – in vivo animal study. *Clin Oral Implants Res*. 2016;27(5):597–603.
24. Kokubo S, Fujimoto R, Yokota S, et al. Bone regeneration by recombinant human bone morphogenetic protein-2 and a novel biodegradable carrier in a rabbit ulnar defect model. *Biomaterials*. 2003;24(9):1643–1651.
25. Leonard D, Buchanan F. The effect of gamma sterilisation on the mechanical properties and bioresorption rate of poly(L-lactide). *7th World Biomaterials Congress 2004*. Available from: http://www.scopus.com/inward/record.url?scp=13844266986&partnerID=8YFLogxK. Accessed September 25, 2017.
26. Saidu MF, Mashita M, Khadijah K, Fazan F, Khalid KA. Sterilisation effect study on granular hydroxyapatite (HA). *Med J Malaysia*. 2004;59(Suppl B):85–86.
27. Russell N, Oliver RA, Walsh WR. The effect of sterilization methods on the osteoconductivity of allograft bone in a critical-sized bilateral tibial defect model in rabbits. *Biomaterials*. 2013;34(33):8185–8194.

28. Godara A, Raabe D, Green S. The influence of sterilization processes on the micromechanical properties of carbon fiber-reinforced PEEK composites for bone implant applications. *Acta Biomater*. 2007;3(2):209–220.
29. Alothman OY, Almajhdi FN, Fouad H. Effect of gamma radiation and accelerated aging on the mechanical and thermal behavior of HDPE/HA nano-composites for bone tissue regeneration. *Biomed Eng Online*. 2013;12:95.
30. Zheng J, Clogston JD, Patri AK, Dobrovolskaia MA, McNeil SE. Sterilization of silver nanoparticles using standard gamma irradiation procedure affects particle integrity and biocompatibility. *J Nanomed Nanotechnol*. 2011;2011(Suppl 5):001.